metals

MDPI

Article

Annealing Response of a Cold-Rolled Binary Al–10Mg Alloy

Lei Feng, Jianguo Li *, Chunfa Huang and Jinxian Huang

School of Material Sciences and Engineering, Tsinghua University, Beijing 100084, China
* Correspondence: jg.li@mail.tsinghua.edu.cn; Tel.: +86-010-62791092

Received: 7 May 2019; Accepted: 3 July 2019; Published: 5 July 2019

Abstract: The effect of annealing temperature on microstructure and mechanical properties of a cold-rolled Al–10Mg alloy has been investigated by X-ray diffraction (XRD), scanning electron microscopy (SEM), electron backscatter diffraction (EBSD) and tensile testing. The results showed that supersaturated Mg precipitated along grain boundaries and deformation bands during annealing treatment and precipitation size and the concentration of solid solution Mg atoms increased with the rising of annealing temperature. When annealed at low temperature, accumulation and annihilation of dislocations were the primary way of recovery; as temperature increased to 300 °C, recrystallized grains were formed around the large size β phase through particle-stimulated nucleation. A high ultimate strength (550 MPa) and a middle ductility (14%) were obtained when the Al–10Mg alloy was annealed at 200 °C for 1 h. The abnormal decrease of elongation when the Al–10Mg alloy was annealed at 250–300 °C was due to the formation of a continuous network distribution of large size β phase particles along grain boundaries.

Keywords: Al–10Mg alloy; β phase; recrystallization; mechanical properties; annealing

1. Introduction

Al–Mg alloys have been extensively used in aerospace, naval ship and automobile manufacturing due to a high specific strength, good corrosion resistance and weld ability [1–4]. However, the strength and ductility of Al–Mg alloys are still not enough for the application in industry. Solid-solution strengthening is often used to increase the strength of Al–Mg series alloy through increasing the content of solute Mg atoms [5,6].

The increase of Mg content in an Al alloy can obviously enhance the strength of it [5,6]. High-magnesium aluminum alloys are non-heat-treatable and are usually used in the cold-rolled or annealed state. A 5083 (~Al–4.5Mg–0.6Mn) alloy annealed at 200 °C obtained a tensile strength of ~450 MPa and an elongation of 13% [7]. An Al–5Mg alloy, which was prepared by equal channel angular extrusion and annealed at 180 °C for 4 h, obtained a higher elongation while maintaining the relative strength of the original alloy [8]. An Al–10Mg alloy sheet achieved a tensile strength of 385 MPa and an elongation of 35% after annealing [9].

However, supersaturated Mg atoms are easily precipitated during heat treatment, which causes changes in the mechanical properties of the alloy. On the one hand, in the annealing of a 5A06 (Al–6.6Mg–0.66Mn) alloy, precipitation of a β (Al_3Mg_2) phase and recrystallization of the structure lead to a decrease in the alloy strength [10]. On the other hand, the elongation of an Al–10Mg alloy was greatly reduced when there was a continuous distribution of β phase in the grain boundaries [11].

Therefore, it is necessary to study the evolution process of β phase in high-magnesium aluminum alloys during annealing and its influence on microstructure and properties. In this article, the effect of annealing temperature on microstructure evolution and mechanical properties will be discussed,

which may lay the theoretical foundation for the future preparation of high magnesium content Al–Mg alloys.

2. Materials and Methods

The material used in this study was produced by centrifugal casting with commercial pure Al (99.7%) and commercial pure Mg. The composition of the alloy, detected by inductively coupled plasma mass spectrometry, is shown in Table 1. Solid solution treatment at 400 °C for 24 h and subsequent water quenching was performed. After the quench, the alloy was hot rolled from 18 to 3 mm with a reduction of 83.3% and cold rolled with reduction of 67.7% to 1 mm. Annealing was carried out at 170–400 °C for 1 h on the cold-rolled alloy.

Table 1. The chemical composition (wt %) of Al–10Mg alloy.

Element	Mg	Fe	Si
Al–10 Mg	9.64	0.117	0.067

To observe the microstructure of the annealed Al–10Mg alloy, optical microscopy, FEI QUANTA-200F scanning electron microscope (SEM, ETH Zurich, Zürich, Switzerland), JEOL JXA8230 electron-probe microanalysis (EPMA, Japan Electronic Co., Ltd. Japan) and electron backscatter diffraction (EBSD, AMETEK, Berwyn, PA, USA) were used. The step size of the EBSD test was 0.15 μm, and scanning data was analyzed by TSL-OIM software (OIM Analysis™ v7.3 AMETEK, Berwyn, PA, USA). The sample used for microstructure investigations were cut from the center of the annealed plate along rolling direction (RD)-normal direction (ND) and were electropolished. Texture and dislocation density were calculated through the result of EBSD. Additionally, the phase structure was detected through X-ray diffraction (XRD) measurements. The scanning rate was 2 °/min and range of 2θ was 30–85°. Because the thickness of the sample in the direction of RD-TD (transverse direction) was thin, the sample for XRD was cut along the RD-TD direction.

Tensile samples with a gauge length of 25 mm and a 7 × 1 mm^2 cross-sectional area were cut from the center of rolled plate parallel to the rolling direction. Tensile tests were conducted at room temperature using a WDW-100 electronic universal testing machine (Shanghai Jingmi Co., Shanghai, China) with a tensile speed of 0.5 mm/min. The elongation of the specimens was measured from the difference in gauge length before and after testing. Strength and ductility shown in this article were an average of three samples.

3. Results

3.1. Effect of Annealing Temperature on Precipitations in Al–10Mg Alloys

X-ray diffraction patterns of the Al–10Mg alloy are shown in Figure 1. The main phase in this alloy was an α-Al phase. At 250–300 °C, another phase whose patterns correspond to the Al_3Mg_2 phase was detected. With the increase of temperature, the amount of β phase increased. However, as the temperature rose to 350 °C, the amount of β phase decreased again due to the increase of solubility of Mg. As reported before, the lattice parameter of Al–Mg alloys increases linearly with the amount of Mg in solid solution (1 at. % Mg resulting in 0.0046 Å increase of α-Al) [2,12]. According to the peak position shown in Figure 1, the concentration of Mg solid solution in α-Al matrix at different annealing temperatures was calculated and shown in Table 2. Besides, the change in intensity ratio between the characteristic Al (220) and (111) lines indicate significant texture changes in the material, and indicate that the material is recrystallized at 350 °C.

Figure 2 shows the microstructure of Al–10Mg cold-rolled sheets annealed at different temperatures for 1 h in an air furnace. Below 200 °C, a large number of submicron-scale needle precipitates were formed, which distributed along grain boundaries and subgrain boundaries. The precipitates were recognized as β' phase, which is a metastable β phase and has a semicoherent lattice with α-Al

matrix [13,14]. In this condition, the matrix contained a large density of dislocations. The β′ phase precipitated from supersaturated station through a process which is facilitated by pipe diffusion via dislocations [15,16]. The growth speed of the β′ phase was faster when nucleated at high-angle grain boundaries [17]. At 250 °C, the scale of the precipitates increased to 1–5 μm and formed a continuous network along grain boundaries and deformation bands. Above 350 °C, the sample was fully recrystallized, and the amount of precipitates decreased because of the redissolution of Mg atoms into the solid solution.

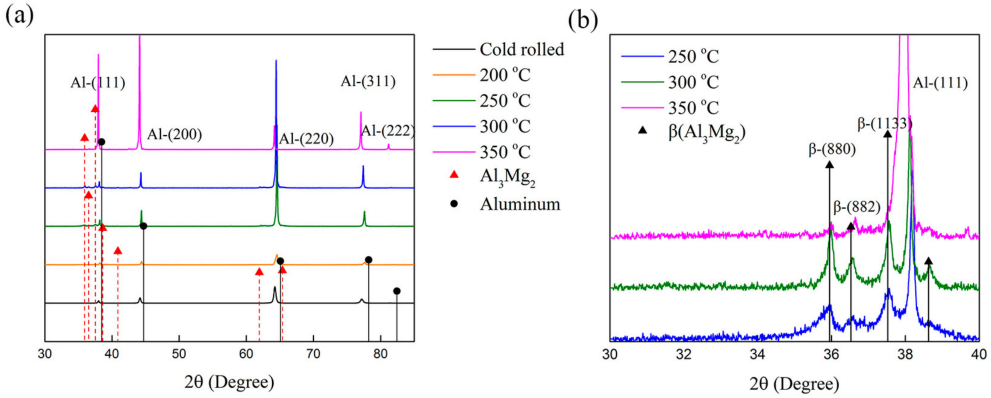

Figure 1. X-ray diffraction (XRD) pattern of Al–10Mg alloy at different states; (**b**) is local amplification of (**a**).

Table 2. Chemical composition (wt %) of Mg atom solute in matrix.

Annealing Temperatures	200 °C	250 °C	300 °C	350 °C
Calculated Mg content	5.16	5.56	7.22	9.33

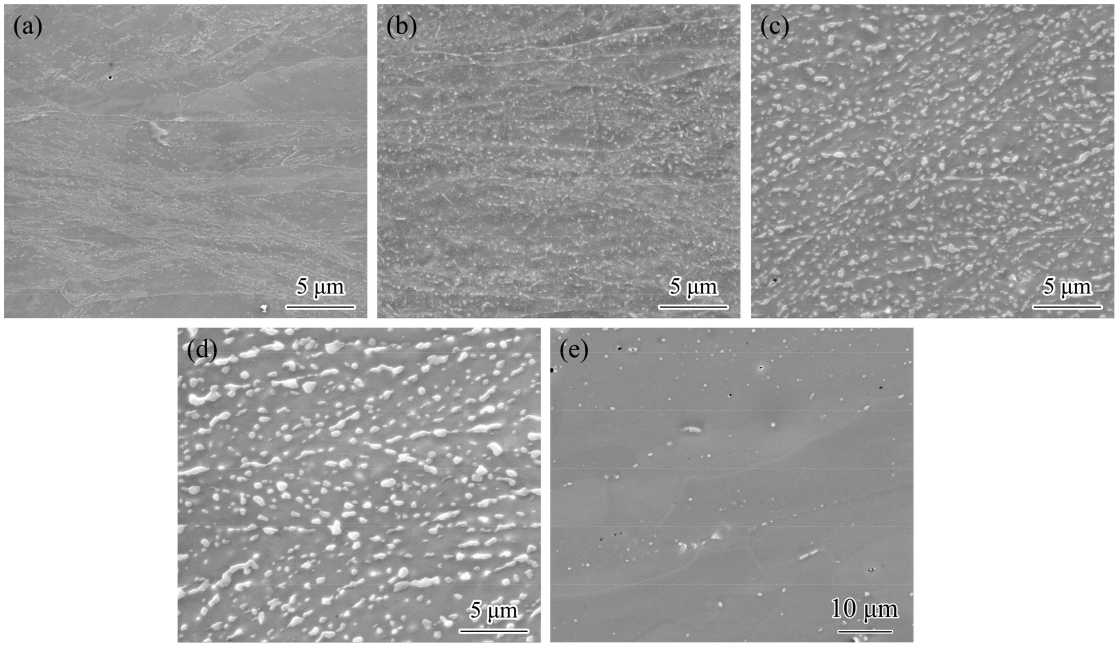

Figure 2. Secondary scanning electron microscopy microstructure of cold-rolled Al–10Mg alloy annealed at (**a**) 70 °C, (**b**) 200 °C, (**c**) 250 °C, (**d**) 300 °C, (**e**) 350 °C for 1 h in an air furnace.

Figure 3 shows the composition mapping of Mg atoms. At 200 °C, Mg atoms were uniformly distributed in the alloy, and β′precipitates caused only lattice distortion within the alloy.

At 300 °C, large-size β precipitates, which caused severe segregation of Mg atoms, formed a network structure distributed along grain boundaries and micro-shear bands. Network structures in grain boundaries dropped the mobility of grain boundaries in the process of tensile deformation and caused uncoordinated deformation between different grains. Also, the stable β phase is a brittle phase, which is incoherent with the matrix, and the phase boundary energy between β phase and the matrix is larger than the grain boundary energy of the Al matrix. So crack sources were easily formed along the phase boundaries under the action of external force during the tensile process, and then caused fractures to the alloy.

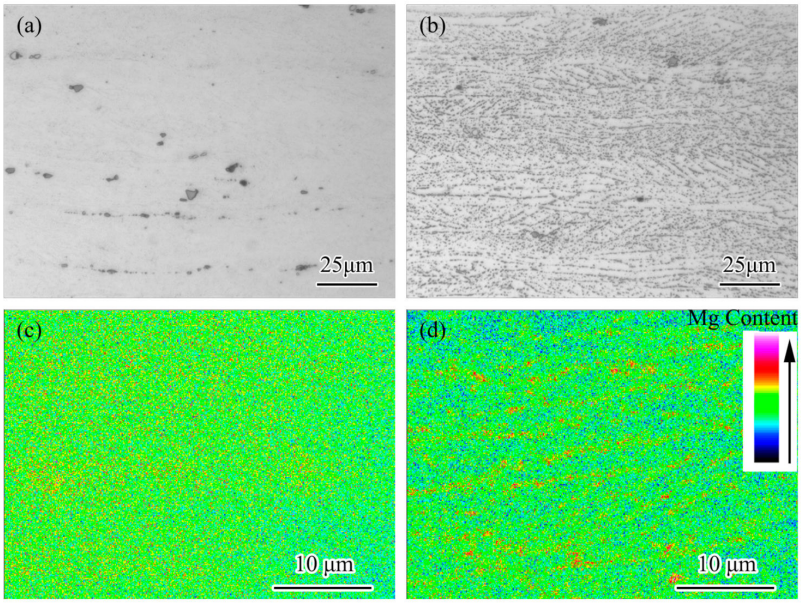

Figure 3. (**a**,**b**) Optical microstructure and (**c**,**d**) element distribution (analyzed by electron-probe microanalysis (EPMA)) of Al–10Mg alloy annealed at (**a**,**c**) 200 °C and (**b**,**d**) 300 °C.

3.2. Effect of Annealing Temperature on Texture

Figure 4 shows the Inverse pole figure (IPF) microstructure and distribution of Orientation distribution function (ODF) intensity of the Al–10Mg alloy annealed at different temperatures. Because of the presence of noise, noise reduction of the microstructure has been carried out. According to the misorientation distribution, dislocation density was estimated with equation $\rho = \theta/\delta b$ [6]. θ was the accumulative misorientation angle in radians within a distance δ, where b is the Burger vector, which is equal to 0.286 nm in aluminum. The calculated results of dislocation density are shown in Table 3. Dislocation density decreases with the rising of annealing temperature.

At 200 °C, the structure has an obvious lamellar structure, which is subdivided by high angle grain boundaries (HAGBs) and extends parallel to RD. A large number of low-angle grain boundaries and deformation bands were present in the microstructure. Dislocations were accumulated along the grain boundaries and micro-shear bands with the increase of annealing temperature. At 300 °C, the lamellar structure become straighter and recrystallized grains occurred at the original grain boundaries. The equiaxed recrystallized grains had an average size of ~5 μm. As the temperature increased to 350 °C, the Al–10Mg alloy was fully recrystallized with a uniform distributed equiaxed grain structure with an average grain size of 30 μm. Solute ability of Mg atoms was enough to dissolve 10 wt % Mg atoms at 400 °C and no more β phase particles appeared.

The general textures observed in face centered cubic (FCC) metals were (i) plane-strain texture components of brass, copper and S; (ii) recrystallized texture component of cube, Goss and P. From the ODF maps, the Al–10Mg alloy have a typical rolling texture before annealing, which have a high content of brass, copper and S texture [18]. At 200 °C (Figure 5), the content of copper and brass texture

decreased and that of S texture increased. This was mainly caused by the formation of the R texture (142)[211], which has a similar orientation as the S texture [19]. This result confirms that the recovery mechanism at this stage was the continuous accumulation and annihilation of dislocations. The texture at 350 °C is hard to interpret (no obvious texture), probably due to poor statistics (based on too few grains), but it is obviously very different from the textures at 200 and 300 °C, consistent with the fact that the material now is recrystallized (cf. Figure 4c).

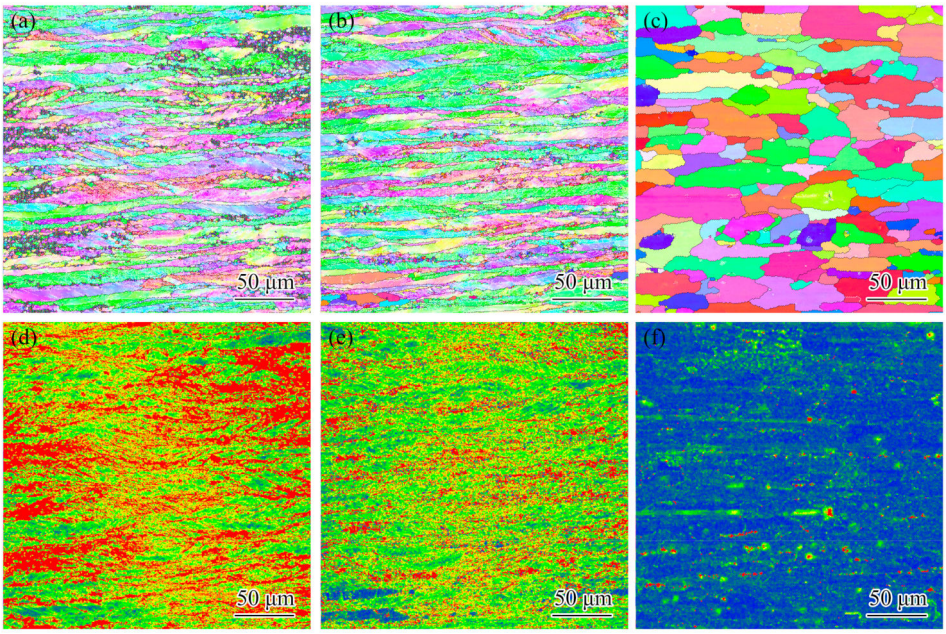

Figure 4. (**a**–**c**) Electron backscatter diffraction (EBSD) orientation micrographs, (**d**–**f**) kernel average misorientation maps of Al–10Mg alloy annealed at (**a**,**d**) 200 °C, (**b**,**e**) 300 °C, (**c**,**f**) 350 °C. Black line in (**a**–**c**) represents misorientation angle θ > 15°. Red regions in (**d**–**f**) represent high misorientation with neighboring points and blue regions represent low misorientation with neighboring points.

Table 3. Dislocation density (m^{-2}) of Al–10Mg alloy annealed at different temperature.

Annealing Temperature	200 °C	300 °C	350 °C
Calculated dislocation density	1.47×10^{13}	5.23×10^{12}	4.11×10^{11}

When the alloy was annealed at 200 °C, the dislocation density and the rolling texture content decreased. However, the alloy had not enough driving force to form any recrystallized grains due to the low annealing temperature. The main microstructure characteristics at this temperature were accumulation and annihilation of dislocations at grain boundaries. Dislocations accumulated in defects and migrated to the high-angle grain boundaries and then merged into them. The formation of R texture at this temperature confirms the recovery of S texture [20,21]. At 300 °C, the structure is still of the fibrous type, however the content of the three main rolling texture components decreased compared to that of the as-rolled alloy. Dislocations within the grains decreased and accumulated along the grain boundaries and micro-shear bands. Recrystallized grains appeared (Figure 4b), but no recrystallization texture was found. Additionally, recrystallized grains mainly distributed along the elongated grain boundaries and at the large-size β phase particles. The presence of large-size β phase particles provides nucleation sites for recrystallized grains and gives rise to discontinuous recrystallization by particle-stimulated nucleation (PSN) [22–25]. So, the primary mechanism of microstructure evolution is the recovery of elongated grains and the formation of recrystallized grains, which nucleated heterogeneously on the surface of β precipitates. The increase of annealing temperature and cocurrent precipitation of β phase changed the mechanism of Al–10Mg alloy recovery

from continuous recovery into discontinuous recrystallization. As annealing temperature increased to 350 °C, a fully recrystallized structure with no distinct texture was obtained (cf. Figures 4c and 5d).

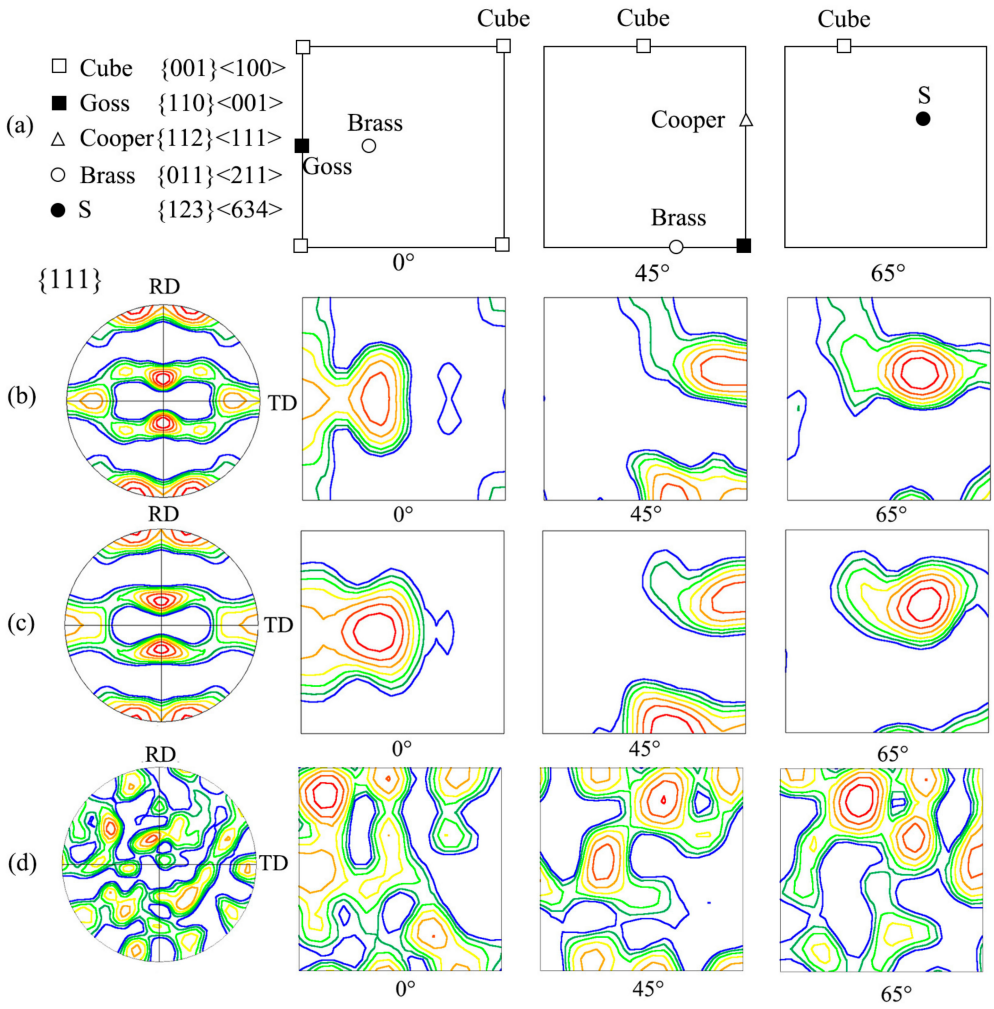

Figure 5. Textures corresponding to the orientation maps presented in Figure 4 in (**b**) 200 °C, (**c**) 300 °C and (**d**) 350 °C. (**a**) shows the ideal texture components of FCC metals [26]. The results were recalculated to the standard rolling direction-transverse direction(RD-TD) coordinated system and presented in the form of the {111} pole figures and the essential part of the orientation distribution function for Ψ2 sections of 0°, 45°and 65°.

3.3. Effect of Annealing Temperature on Mechanical Properties

Engineering stress-strain curves of Al–10Mg alloy annealed at different temperatures are shown in Figure 6. With the increase of temperature, the yield and ultimate strength of the Al–10Mg alloy decreased. The main reason for the decrease of strength consisted of two parts: On the one hand, with the increase of annealing temperature, dislocation density decreased, and recovery and recrystallization occurred in the Al–10Mg alloy. On the other hand, concurrent precipitation of β phase reduced the Mg content solute in the matrix and then weakened the effect of solid–solution strengthening. Notably, the cold-rolled state of the Al–10Mg alloy obtained a high strength (ultimate strength (UTS): 580 MPa) and a middle ductility (elongation (EI): 8.5%). After annealing at 200 °C, the alloy obtained an excellent combination of strength (UTS: 550 MPa) and ductility (EI: 14%), which is similar to that of a similar alloy produced by severe plastic deformation.

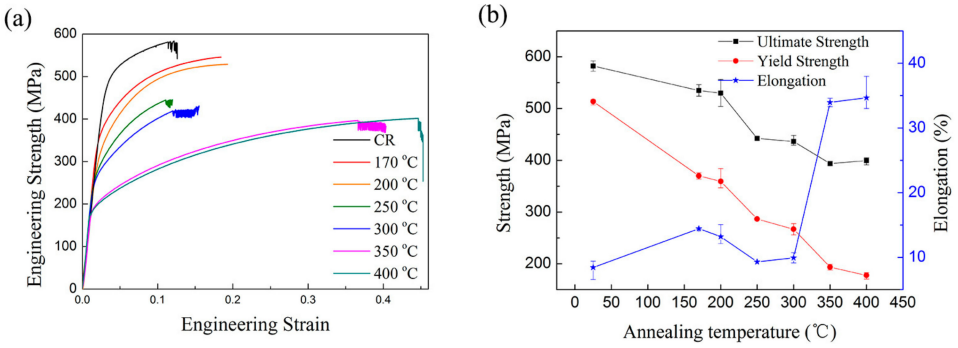

Figure 6. Typical (**a**) engineering stress–strain curves and evolution (**b**) of mechanical properties of Al–10Mg alloy sheet annealed at different temperatures.

Another interesting observation in this alloy was the serrations that appeared after yielding. Serrations, which is related to dynamic strain aging (DSA), is the result of interaction between solute atoms and dislocations [27]. Strength increased as the DSA effect occurred in the tensile tests when the diffusion rate of solution atoms was higher than the movement rate of dislocations. Serrations was observed in almost all the states except the alloy annealed at 170 and 200 °C. At these temperatures, the content of the solid solution Mg atoms has decreased to 5.16 wt %; dislocation density was still more prominent than that under normal conditions. The pinning effect of Mg atoms on dislocations was too small to induce any DSA effect [28,29]. With the increase of annealing temperature, Mg content increased, and dislocation density decreased, the amount of mobile dislocations increased, and then the effect of DSA increased. However, it was detrimental to the formability of alloy for forming early necking and fracture.

In conventional Al–Mg alloys, elongation increases with an increasing annealing temperature [30]. However, an abnormal drop occurred in ductility of the present alloy that annealed at 250–300 °C. There are two possible reasons why an abnormal decline occurred to elongation of the Al–10Mg alloy annealed at 250–300 °C. First, the mechanism of alloy recovery and recrystallization was not the same at different annealing temperatures, which resulted in different internal texture, thus resulting in different elongations of the alloy. Secondly, the size and distribution of β phase have different effects on the elongation of the alloy. Now, a detailed analysis of these two mechanisms will be done.

The first was the impact of grain orientations on elongation under different annealing conditions. The deformation direction paralleled to the RD direction when the sample was stretched. The orientation distribution of the samples in the TD-ND plane, i.e., along the RD direction is shown in Figure 7. Texture intensity and Schmid factors of the 12 normal slip systems in FCC metals were calculated from the result of inverse pole figures. According to the inverse pole figure, the preferred orientations has no big change at 200 and 300 °C. This indicates grain orientation is not the main reason for the elongation drop when annealing at 300 °C. As temperature increased to 350 °C, the preferred orientations changed completely (cf. Figure 7c vs. Figure 7b) and the <104> direction became the preferred orientation, which highest Schmid factor is 0.48. This indicates the {104} orientated grains can fully slip in the deformation process so that the alloy would have a relatively good deformation ability. And the alloy annealed at 350 °C can obtain a higher elongation.

Another reason was the concurrent precipitation of β phase. Figure 8 shows the fracture morphology of the Al–10Mg alloy annealed at different temperatures. In the cold-rolled state, the alloy has a lamellar fracture, which is associated with the fibrous structure of the cold-rolled alloy. At 200 °C, dimples with a diameter of 1 μm occurred, and no precipitates were found in the dimples. This observation indicates that the precipitate β′ phase had no significant influence on elongation. Additionally, a cracked second phase was found in the fracture surface. As temperature increased to 300 °C, the fracture is changed into dimple rupture, and the dimple is only 1 μm in size. β phase particles, which have a similar size, were observed in the dimples. In the process of stretching,

the interface between the brittle concurrent β phase and the matrix was straightforward to crack under the action of an external force, forming a crack source, and ultimately caused a significant decrease in the elongation of the alloy. Additionally, large cracked β phase particles, which were formed in the original microstructure and have no relationship with the annealing process, were founded in this condition. As the temperature increased to 400 °C, the size of dimple increased to 20 μm, no β phase was found in the dimple and the alloy had a good ductility.

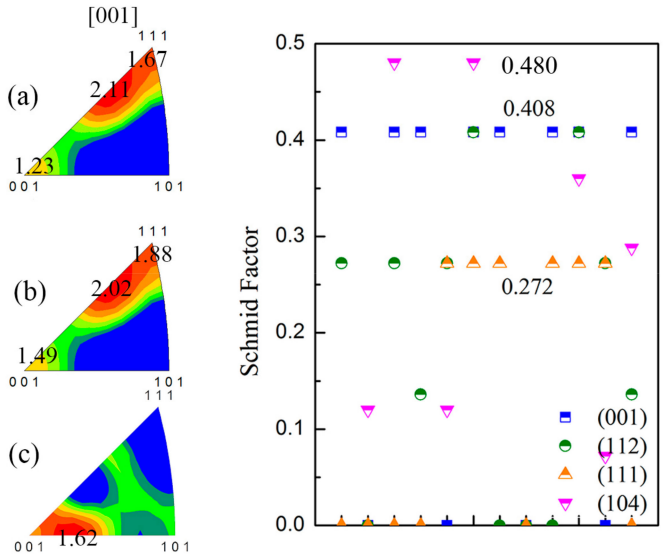

Figure 7. Inverse pole figure of RD direction and corresponding Schmid factor of Al–10Mg alloy along TD-ND plane annealed at (**a**) 200 °C, (**b**) 300 °C and (**c**) 350 °C.

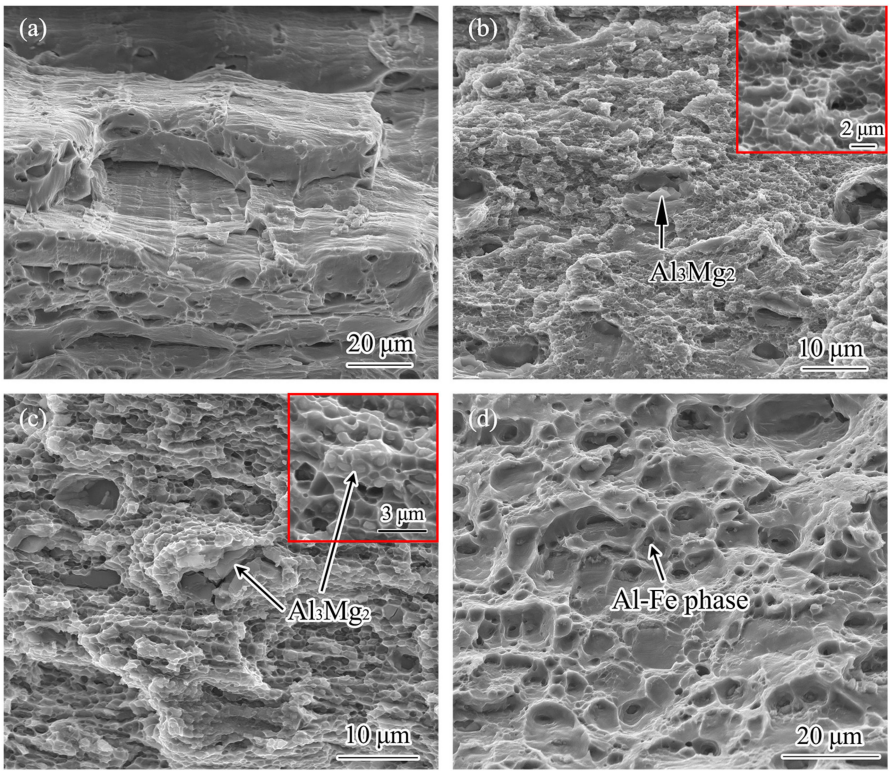

Figure 8. Secondary SEM fracture morphology of Al–10Mg alloy annealed at (**a**) cold-rolled, (**b**) 200 °C, (**c**) 300 °C and (**d**) 400 °C.

4. Conclusions

(1) Precipitates formed along grain boundaries and deformation bands during annealing of an Al–10Mg alloy, and the main formation mechanism was dislocation-controlled channel diffusion. With the increase of annealing temperature, precipitation change from needle-like submicro-sized β' phase into larger-size stable β phase, while the solubility of Mg in the matrix increased. The increase of annealing temperature enhanced the DSA effect through the solid solution of Mg atom and the higher mobility of dislocations.

(2) The initial temperature of recrystallization of the alloy was 300–350 °C. At 200 °C, the Al–10Mg alloy recovered through accumulation and annihilation of dislocations; at 300 °C, recrystallized grains heterogeneous nucleated at large-size β phase particles, which precipitated along the elongated grain boundaries.

(3) The Al–10Mg alloy obtained a high ultimate strength of 550 MPa and a middle elongation of 14% through traditional rolling and annealing (200 °C) processes. Dislocation density and strength of alloy decreased when the annealing temperature increased. The elongation decreased at 300 °C, mainly due to the existence of large-size β phase particles continuously distributed along the grain boundaries.

Author Contributions: L.F. and J.L. conceived and designed the experiments; L.F. performed the experiments; L.F. analyzed the data; L.F., C.H and J.H. contributed materials/analysis tools; L.F. and J.L. wrote the paper.

Funding: This research was funded by Tsinghua University Initiative Scientific Research Program grant No.20173080030 and The ISTCP grant No.2015DFR50470.

Conflicts of Interest: The authors declare no conflicts of interest.

References

1. Toros, S.; Ozturk, F.; Kacar, I. Review of warm forming of aluminum–magnesium alloys. *J. Mater. Process. Tech.* **2008**, *207*, 1–12. [CrossRef]
2. Zha, M.; Li, Y.; Mathiesen, R.H. Achieve high ductility and strength in an Al-Mg alloy by severe plastic deformation combined with inter-pass annealing. *Mater. Sci. Eng. A* **2014**, *598*, 141–146. [CrossRef]
3. Kendig, K.L.; Miracle, D.B. Strengthening mechanisms of an Al-Mg-Sc-Zr alloy. *Acta Mater.* **2002**, *50*, 4165–4175. [CrossRef]
4. Mikhaylovskaya, A.; Kotov, A.; Kishchik, M.; Prosviryakov, A.; Portnoy, V. The Effect of Isothermal Multi-Directional Forging on the Grain Structure, Superplasticity, and Mechanical Properties of the Conventional Al–Mg-Based Alloy. *Metals* **2019**, *9*, 33. [CrossRef]
5. Bo, W.; Chen, X.; Pan, F.; Mao, J.; Yong, F. Effects of cold rolling and heat treatment on microstructure and mechanical properties of AA 5052 aluminum alloy. *Trans. Nonferr. Metal. Soc.* **2015**, *25*, 2481–2489.
6. Zha, M.; Meng, X.T.; Zhang, H.M.; Zhang, X.H.; Jia, H.L.; Li, Y.J.; Zhang, J.Y.; Wang, H.Y.; Jiang, Q.C. High strength and ductile high solid solution Al-Mg alloy processed by a novel hard-plate rolling route. *J. Alloys Compd.* **2017**, *728*, 872–877. [CrossRef]
7. Lee, Y.B.; Shin, D.H.; Park, K.T. Effect of annealing temperature on microstructures and mechanical properties of a 5083 Al alloy deformed at cryogenic temperature. *Scr. Mater.* **2004**, *51*, 355–359. [CrossRef]
8. Snopinski, P.; Król, M. Microstructure, Mechanical Properties and Strengthening Mechanism Analysis in an AlMg5 Aluminium Alloy Processed by ECAP and Subsequent Ageing. *Metals* **2018**, *8*, 969. [CrossRef]
9. Lee, B.H.; Kim, S.H.; Park, J.H. Role of Mg in simultaneously improving the strength and ductility of Al-Mg alloys. *Mater. Sci. Eng. A* **2016**, *657*, 115–122. [CrossRef]
10. Ma, B.X.; Wang, G.J.; Guo, E.J. Effect of annealing temperature on microstructure and tensile properties of Al–Mg alloy 5A06 sheet. *Mater. Sci. Technol.* **2013**, *29*, 1044–1047. [CrossRef]
11. Mcnelley, T.R.; Garg, A. Development of structure and mechanical properties in Al-10.2 WT. PCT. Mg by thermomechanical processing. *Scr. Mater.* **1984**, *18*, 917–920. [CrossRef]
12. Valiev, R.Z.; Enikeev, N.A.; Murashkin, M.Y. On the origin of the extremely high strength of ultrafine-grained Al alloys produced by severe plastic deformation. *Scr. Mater.* **2010**, *63*, 949–952. [CrossRef]
13. Bensaada, S.; Bouziane, M.T.; Mohammedi, F. Effect of the temperature on the mechanism of the precipitation in Al-8% mass.Mg alloy. *Mater. Lett.* **2011**, *65*, 2829–2832. [CrossRef]

14. Yi, G.; Cullen, D.A. Characterization of Al-Mg Alloy Aged at Low Temperatures. *Metall. Mater. Trans. A* **2017**, *48*, 2040–2050. [CrossRef]
15. Goswami, R.; Spanos, G.; Pao, P.S. Precipitation behavior of the β phase in Al-5083. *Mater. Sci. Eng. A* **2010**, *527*, 1089–1095. [CrossRef]
16. D'Antuono, D.S.; Gaies, J.; Golumbfskie, W. Direct measurement of the effect of cold rolling on β phase precipitation kinetics in 5xxx series aluminum alloys. *Acta Mater.* **2017**, *123*, 264–271.
17. D'Antuono, D.S.; Gaies, J.; Golumbfskie, W. Grain boundary misorientation dependence of β phase precipitation in an Al–Mg alloy. *Scr. Mater.* **2014**, *76*, 81–84. [CrossRef]
18. Miszczyk, M.M.; Paul, H.; Driver, J.H.; Poplewska, J. The influence of deformation texture on nucleation and growth of cube grains during primary recrystallization of AA1050 alloy. *Acta Mater.* **2017**, *129*, 178–387. [CrossRef]
19. Liu, J.; Banovic, S.W.; Biancaniello, F.S.; Jiggetts, R.D. Through-thickness texture gradient in an annealed Al-Mg alloy sheet. *Met. Mater. Trans. A* **2005**, *36*, 869–874. [CrossRef]
20. Gatti, J.R.; Bhattacharjee, P.P. Microstructure and Texture of Al-2.5wt.% Mg Processed by Combining Accumulative Roll Bonding and Conventional Rolling. *J. Mater. Eng. Perform.* **2014**, *23*, 4453–4462. [CrossRef]
21. Gatti, J.R.; Bhattacharjee, P.P. Annealing textures of severely cold and warm-rolled Al–2.5wt.% Mg alloy. *J. Alloy. Compd.* **2014**, *615*, 950–961. [CrossRef]
22. Ihara, K.; Oga, H.; Miura, Y. Interaction between moving boundaries and Al_3Sc precipitates in an Al-5 mass% Mg-0.3 mass% Sc alloy. *J. Jpn. Inst. Light Met.* **2006**, *56*, 361–365. [CrossRef]
23. Humphreys, F.J. The nucleation of recrystallization at second phase particles in deformed aluminium. *Acta Metall.* **1977**, *25*, 1323–1344. [CrossRef]
24. Kang, J.; Wilkinson, D.S.; Jain, M. On the sequence of inhomogeneous deformation processes occurring during tensile deformation of strip cast AA5754. *Acta Mater.* **2006**, *54*, 209–218. [CrossRef]
25. Yizhe, M.; Jianguo, L.; Lei, F. Effect of Coarse β(Al_3Mg_2) Phase on Microstructure Evolution in 573 K Annealed Al-10Mg Alloy by Uniaxial Compression. *Acta Met. Sin.* **2018**, *54*, 1451–1460.
26. Yang, H.W.; Widiantara, I.P.; Joo, Y.H. Effect of deformation path on texture and tension properties of submicrocrystalline Al-Mg-Si alloy fabricated by differential speed rolling. *Mater. Lett.* **2018**, *213*, 54–57. [CrossRef]
27. Zha, M.; Li, Y.J.; Mathiesen, R.H.; Baumgart, C.; Roven, H.J. Influence of Mg Content, Grain Size and Strain Rate on Mechanical Properties and DSA Behavior of Al-Mg Alloys Processed by ECAP and Annealing. *Mater. Sci. Forum.* **2014**, *794*, 870–875. [CrossRef]
28. Robinson, J.M. In-situ deformation of aluminium alloy polycrystals observed by high-voltage electron microscopy. *Mater. Sci. Eng. A* **1995**, *203*, 238–245. [CrossRef]
29. Xiao, L.G.; Li, X.Q.; Jian, K.W. A model for the occurrence of serrated yielding in substitutional alloys. *Sci. China Math.* **1990**, *33*, 1386–1396.
30. Avtokratova, E.; Sitdikov, O.; Mukhametdinova, O. Microstructural evolution in Al–Mg–Sc–Zr alloy during severe plastic deformation and annealing. *J. Alloy. Compd.* **2016**, *673*, 182–194. [CrossRef]